JOC The Journal of Organic Chemistry

Article

pubs.acs.org/joc

Cooperativity and Site-Selectivity of Intramolecular Hydrogen Bonds on the Fluorescence Quenching of Modified GFP Chromophores

Deng-Hsiang Chang,[†] Chun-Lin Ou,[†] Hung-Yu Hsu,[‡] Guan-Jhih Huang,[†] Chen-Yi Kao,[†] Yi-Hung Liu,[†] Shie-Ming Peng,[†] Eric Wei-Guang Diau,[‡] and Jye-Shane Yang*[,†]

[†]Department of Chemistry, National Taiwan University, Taipei 10617, Taiwan

[‡]Department of Applied Chemistry and Institute of Molecular Science, National Chiao Tung University, Hsinchu 30010, Taiwan

Supporting Information

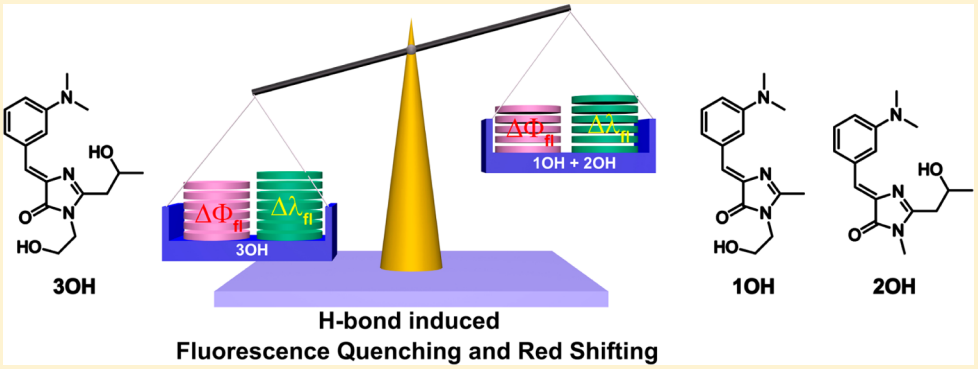

ABSTRACT: This paper provides the first example of experimentally characterized hydrogen-bond cooperativity on fluorescence quenching with a modified green fluorescence protein (GFP) chromophore that contains a 6-membered C═N···H−O and a 7-membered C═O···H−O intramolecular H-bonds. Variable-temperature ^{1}H NMR and electronic absorption and emission spectroscopies were used to elucidate the preference of intra- vs intermolecular H-bonding at different concentrations (1 mM and 10 μM), and X-ray crystal structures provide clues of possible intermolecular H-bonding modes. In the ground state, the 6-membered H-bond is significant but the 7-membered one is rather weak. However, fluorescence quenching is dominated by the 7-membered H-bond, indicating a strengthening of the H-bond in the excited state. The H-bonding effect is more pronounced in more polar solvents, and no intermediates were observed from femtosecond fluorescence decays. The fluorescence quenching is attributed to the occurrence of diabatic excited-state proton transfer. Cooperativity of the two intramolecular H-bonds on spectral shifts and fluorescence quenching is evidenced by comparing with both the single H-bonded and the non-H-bonded counterparts. The H-bond cooperativity does not belong to the conventional patterns of σ- and π-cooperativity but a new type of polarization interactions, which demonstrates the significant interplay of H-bonds for multiple H-bonding systems in the electronically excited states.

INTRODUCTION

Hydrogen bond plays a critical role in the structures and properties of numerous molecular, supramolecular, and polymeric systems.[1−3] Understanding the H-bonding behavior of these systems is essential for effective application and modification of their properties. Compared to ground-state H-bonds, much less is known about electronic excited-state H-bonding characteristics. H-bonding interactions in the excited state could alter the fluorescence color and intensity and[12,13] trigger the occurrence of proton and/or electron transfer, depending on the nature of chromophore and H-bonding mode.[4−12] For a system containing multiple H-bonding sites, the questions as to whether the H-bonding effects are additive in the excited state and to which H-bonding mode dominates the excited-state behavior are raised. However, these issues have been rarely addressed, not to mention experimental verification of theories or models.

Benzylidenedimethylimidazolinone (BDI) derivatives have attracted much attention because of the intriguing photoluminescence properties of green fluorescent protein (GFP) and its chromophore *p*-hydroxybenzylidenedimethylimidazolinone (*p*-HBDI, Chart 1). Whereas GFP displays strong green fluorescence with a quantum efficiency (Φ_f) near 0.80, the fluorescence of *p*-HBDI is blue and very weak ($\Phi_f < 10^{-3}$) in nonviscous solutions.[14−16] The fluorescence quenching of *p*-HBDI results from ultrafast (subpicoseconds) torsional motions of the exocyclic C═C bond (the τ torsion), which is largely inhibited by the protein matrix in GFP.[17−19] The green fluorescence of GFP is from the anionic form of *p*-HBDI, the formation of which involves a cascade proton transfer triggered by excited-state proton transfer (ESPT) of the

Received: October 4, 2015
Published: November 19, 2015

DOI: 10.1021/acs.joc.5b02303
J. Org. Chem. 2015, 80, 12431−12443

Chart 1

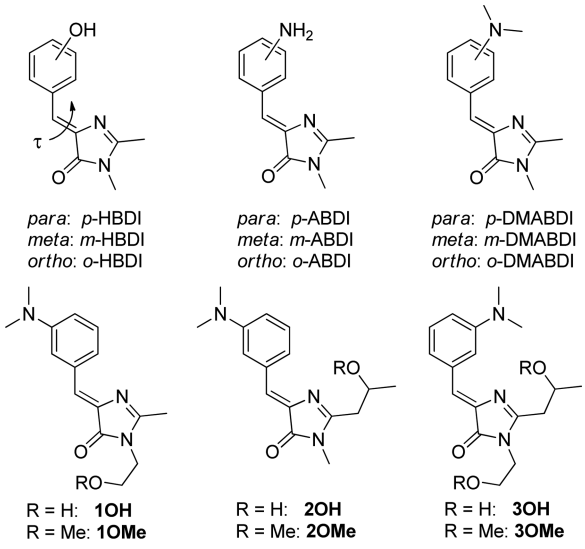

phenolic proton to the H-bonded water molecule.[15,20,21] Without the protein matrix, the ESPT cannot compete with the τ torsion in aqueous solutions. In contrast, ESPT dominates the excited-state deactivation of the *meta* isomer *m*-HBDI because of its slow τ torsion.[22,23] For the *ortho* isomer *o*-HBDI, an intramolecular version of ESPT takes place and leads to fluorescence from the tautomer.[24−26] Besides the HBDI systems, the amino analogs, that is, *p*-, *m*-, and *o*-ABDI, also display intriguing position-dependent photoluminescence properties.[19,27−29] In particular, the *meta*-amino systems, *m*-ABDI and its dimethylamino derivative *m*-DMABDI, display unprecedentedly high Φ_f in aprotic solvents (e.g., Φ_f = 0.46 for *m*-DMABDI in hexane) for structurally unconstrained BDI chromophores.[19,30,31] The fluorescence is however nearly quenched in protic solvents (e.g., $\Phi_f < 10^{-3}$ in CH_3OH) as a result of solvent−solute H-bonding interactions.

In a recent preliminary report,[30] we investigated the site-specific intramolecular H-bonding systems **1OH** and **2OH** to identify the H-bonding mode that is responsible for the fluorescence quenching of *m*-DMABDI in protic solvents. Although DFT calculations predicted a weaker H-bond for the 7-membered C═O···H−O in **1OH** (2.49 kcal mol^{-1}) than the 6-memebered C═N···H−O in **2OH** (5.72 kcal mol^{-1}) in the ground state, the fluorescence quenching is much more significant for the former relative to the non-H-bonded counterparts **1OMe** and **2OMe**, indicating that the C═O···H−O H-bond is strengthened and dominates the observed H-bonding effect in the excited state. The observation of a larger extent of fluorescence quenching in acetonitrile than in hexane indicates an ESPT mechanism, as the zwitterionic product would be better stabilized in more polar solvents. In the current work, the H-bonding behavior of **1OH** and **2OH** in solutions has been further characterized by variable-temperature ^{1}H NMR and electronic absorption and fluorescence spectroscopies.

We also envisioned that the double intramolecular H-bonding system **3OH**, which is an integrate of **1OH** and **2OH**, provides a unique opportunity for addressing the cooperativity of the two H-bonds in the excited state as well as in the ground state. Therefore, **3OH** and the non-H-bonded reference compound **3OMe** have been synthesized and the H-bonding behavior of **3OH** relative to **1OH** and **2OH** in solutions as well as in the solid state has been investigated. The results reported herein confirm that the intramolecular 6-membered C═N···H−O H-bond is much more important than the 7-membered C═O···H−O counterpart in the ground state but the latter plays a greater role in the fluorescence quenching. A cooperative effect of these two bonds in **3OH** is noticeable in the ground state and becomes more significant in the excited state. The concentration, temperature, and solvent effects on intra- vs intermolecular H-bonding interactions and the mechanism of fluorescence quenching are discussed.

RESULTS

Synthesis. The syntheses of **1OH**, **2OH**, **1OMe**, and **2OMe** have been reported,[30] and the same protocols were adopted to prepare **3OH** and **3OMe** from **1OMe** (Scheme 1).

Scheme 1

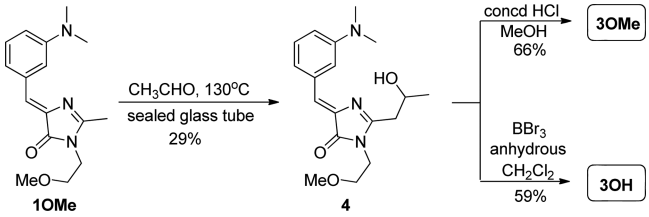

Briefly, the reaction between **1OMe** and acetaldehyde in a sealed glass tube afforded the intermediate **4**; subsequent demethylation of the methoxy group or methylation of the hydroxyl group in **4** led to the target compounds **3OH** and **3OMe**, respectively.

X-ray Crystal Structures. The X-ray crystal structures of **1OH**−**3OH** are shown in Figure 1. Some analogies and

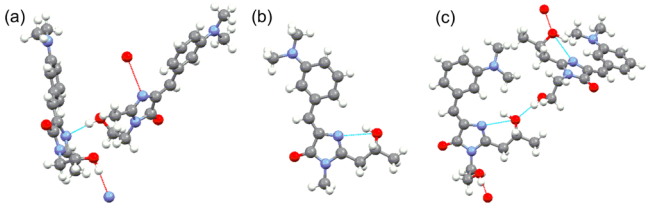

Figure 1. X-ray crystal structures of (a) **1OH**, (b) **2OH**, and (c) **3OH** showing the intra- and/or intermolecular H-bonds.

differences among them are noted. First, the BDI moiety is essentially coplanar for all three cases, although the dihedral angle between the phenyl and the imidazolinone rings is slightly larger for **1OH** (11.8°) than for **2OH** (3.7°) and **3OH** (1.2°). Second, the *N*,*N*-dimethylamino group exhibits a *syn* orientation with respect to the C═O group in both **1OH** and **2OH**, but it is an *anti* form in **3OH**. Third, the hydroxyl group in **1OH** and **2OH** participates in *inter*- and *intramolecular* C═N···H−O H-bonding, respectively. While the **2OH**-like hydroxyl group in **3OH** also adopts an intramolecular C═N···H−O H-bond, the other hydroxyl group adopts an intermolecular H−O···H−O H-bond. Finally, the N-to-O distance in the intermolecular C═N···H−O H-bond in **1OH** is 2.91 Å, which is significantly larger than the intramolecular counterparts in **2OH** (2.82 Å) and **3OH** (2.79 Å). These N-to-O distances are shorter than the van der Waals distance (3.07 Å) by 0.16, 0.25, and 0.28 Å, respectively, for the compound series **1OH**−**3OH**. The O-to-O distance in the intermolecular

DOI: 10.1021/acs.joc.5b02303
J. Org. Chem. 2015, 80, 12431−12443

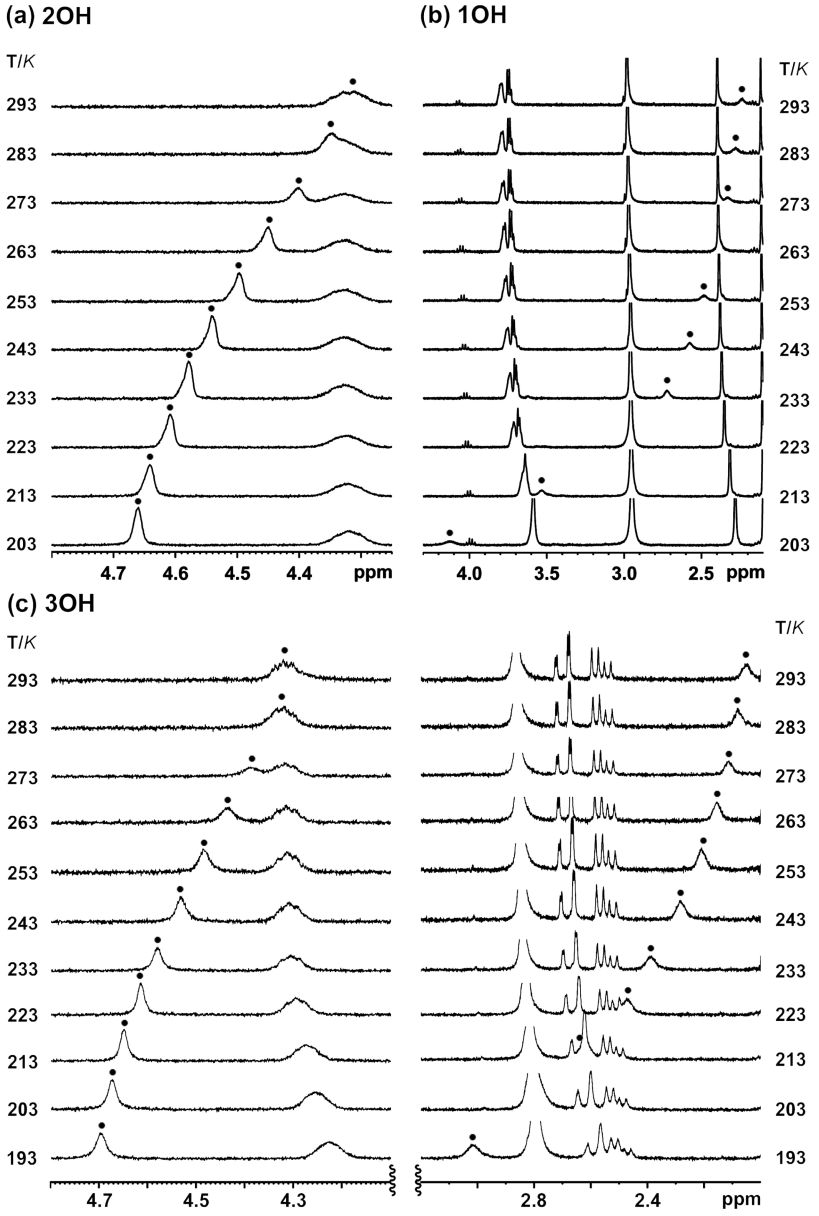

Figure 2. Hydroxyl proton region of VT ^{1}H NMR spectra of (a) **2OH**, (b) **1OH**, and (c) **3OH** in CD_2Cl_2 (1×10^{-3} M) in the range 203−293 or 193−293 K with an interval of 10 K. The solid circles denote peaks due to the hydroxyl proton.

H−O···H−O H-bond of **3OH** is 2.75 Å, which follows the optimal distance of 2.8 Å observed for intermolecular H-bonds in crystals[32] and is shorter than the van der Waals distance (3.04 Å) by 0.29 Å. Interestingly, the arrangement of C═N···H−O···H−O in **3OH** conforms to the pattern of σ-cooperativity of H-bonds,[1] which is consistent with the relatively shorter contacts for **3OH** vs **1OH** and **2OH**. Such a cooperative effect of H-bonds in **3OH** might account for the lack of participation of the carbonyl group in either inter- or intramolecular H-bonding.

Variable-Temperature ^{1}H NMR. Variable-temperature (VT) ^{1}H NMR spectroscopy has been a useful tool for characterizing intra- vs intermolecular H-bonds and for obtaining the thermodynamic information about the equilibrium of the H-bonded (HB) and non-H-bonded (NHB) states in solutions.[32−35] In general, the dependence of chemical shift on temperature, as expressed by reduced temperature constant ($-\Delta\delta/\Delta T$), is small (e.g., < 10 ppb K^{-1} for amide protons in CD_2Cl_2) for an intramolecular H-bond but significant (>10 ppb K^{-1}) for an intermolecular counterpart. For a two-state system with an equilibrium constant K = [HB]/[NHB], the relationships among K, temperature (T), the observed chemical shift (δ_{obs}), chemical shifts of HB (δ_{HB}) and NHB (δ_{NHB}), Gibbs free energy (ΔG), enthalpy (ΔH), and entropy (ΔS) are described by eqs 1-4:

$$\delta_{obs} = [HB]/([HB] + [NHB]) \times \delta_{HB} + [NHB]/([HB] + [NHB]) \times \delta_{NHB} \quad (1)$$

$$=(\delta_{NHB} + \delta_{HB} \times K)/(1 + K) \quad (2)$$

$$=(\delta_{NHB} + \delta_{HB} \times \exp(-\Delta G/RT))/(1 + \exp(-\Delta G/RT)) \quad (3)$$

DOI: 10.1021/acs.joc.5b02303
J. Org. Chem. 2015, 80, 12431−12443

$$=(\delta_{NHB} + \delta_{HB} \times \exp(\Delta S/R) \times \exp(-\Delta H/RT))$$
$$/(1 + \exp(\Delta S/R) \times \exp(-\Delta H/RT)) \quad (4)$$

Nonlinear fitting of the plots of δ_{obs} against T with eq 4 would provide the values of δ_{HB}, δ_{NHB}, ΔG, ΔH, and ΔS.

The VT ^{1}H NMR spectra for **1OH**−**3OH** in CD_2Cl_2 (1×10^{-3} M) show an explicit dependence of the hydroxyl protons on temperature (Figure 2). Upon lowering the temperature, all four hydroxyl protons undergo a dramatic downfield shift. While the downfield shift is accompanied by peak broadening in the case of **1OH**, the signal becomes sharper for **2OH**. Evidently, the H-bonding nature in these two systems is different. Note that the vicinal proton of the OH in **2OH** has a rather broad signal at all the temperatures, and it merges with the signal of OH at 293 K. The two hydroxyl groups in **3OH** retain the features of the corresponding OH in **1OH** and **2OH**. Because of an accidental signal overlapping for the **1OH**-like OH group with the *N*-methyl protons at 203 K, the spectrum of **3OH** at 193 K was also recorded to get a clear picture on the temperature effect.

Figure 3 shows the plots of chemical shift against temperature for the hydroxyl protons of **1OH**−**3OH**, and the corresponding fitting data with eq 4 are listed in Table 1. The nonlinear relationship for all four OH groups indicates that the H-bonding is neither purely intramolecular nor purely intermolecular within the temperature frame. It is also noted that the curvature is upward in **1OH** but downward in **2OH** and so are the corresponding hydroxyl protons in **3OH**. An upward curve means an increase of the $-\Delta\delta/\Delta T$ value upon lowering the temperature, and the opposite is true for a downward curve. Since the size of $-\Delta\delta/\Delta T$ at low temperature (e.g., 193−243 K) reflects the inherent preference of a H-bond being inter- or intramolecular, the data reveal that an intermolecular H-bond is more favorable for **1OH** but an intramolecular version is preferred by **2OH**. The low-temperature $-\Delta\delta/\Delta T$ value for the **2OH**-like OH in **3OH** (designated as **3OH**(2)) is similar to that of **2OH** (3.2 vs 2.9 ppb K^{-1}), but it is much lower (15 vs 39 ppb K^{-1}) for the **1OH**-like OH in **3OH** (designated as **3OH**(1)) than the case of **1OH**. The latter indicates of different intermolecular H-bonding modes.

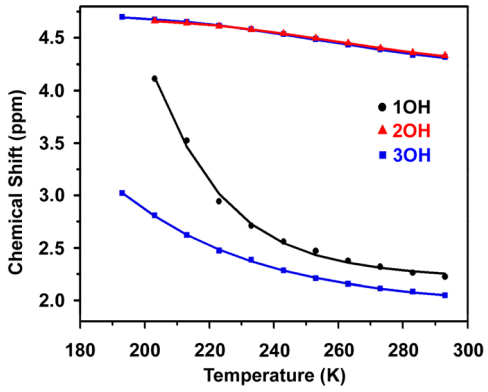

Figure 3. Plots of chemical shift (ppm) against temperature (K) for the hydroxyl protons of **1OH**−**3OH** in CD_2Cl_2 (1×10^{-3} M) in the range of 193−293 K. The regression fitting curves are based on eq 4.

Electronic Absorption Spectra. Figure 4 shows the normalized absorption spectra of **1OH**−**3OH** relative to the corresponding non-H-bonded species **1OMe**−**3OMe** in hexane (1×10^{-5} M). Pertinent spectroscopic data in hexane, THF, and MeCN are provided in Table 2. All the spectra feature an intense band and a long-wavelength shoulder with maxima (λ_{abs}) at ∼350 and ∼430 nm, respectively. The former band could be attributed to a localized π,π^* transition in the BDI moiety, and the latter band to a charge transfer from the dimethylamino donor to the BDI acceptor.[28] The negligible difference in the long-wavelength onset between **1OH** and **1OMe** indicates a rather weak intramolecular C═O···H−O bonding in the former. In contrast, the obvious red shift at the onset of absorption spectra for **2OH** and **3OH** relative to **2OMe** and **3OMe** can be attributed to the intramolecular C═N···H−O bonding. The spectral similarities for **2OH** and **3OH** reveal that the ground-state C═O···H−O H-bond in **3OH** is also weak. When the solvent was replaced with MeCN, all three systems **1OH**−**3OH** display nearly the same absorption spectra (Figure S1), and the spectral onsets coincide with those of the non-H-bonded counterparts **1OMe**−**3OMe**, indicating that the C═N···H−O H-bond is no longer favorable in polar solvents.

To investigate the temperature effect on the H-bonding behavior at the concentration of 1×10^{-5} M, we recorded the absorption spectra of **1OH**−**3OH** and **1OMe**−**3OMe** in methylcyclohexane (MCH) in the temperature range 128−298 K with an interval of 10 K (Figure 5). The measurements ended at 128 K before MCH is frozen into a solvent glass.

Table 1. Thermodynamic and NMR Data for the H-Bonding of 1OH−3OH in CD_2Cl_2 (1×10^{-3} M) Derived with Eq 4

compd	$-\Delta\delta/\Delta T$ (ppb K^{-1})	δ_{HB}[a] (ppm)	δ_{NHB}[a] (ppm)	ΔH (kcal mol^{-1})	ΔS (cal mol^{-1} K^{-1})	$\Delta G_{298\ (193\ K)}$ [b](kcal mol^{-1})	$[HB]_{298\ (193\ K)}$ [b] (%)
1OH	39 (203−243) 6.8 (243−293)	7.87	2.19	−5.01	−25.9	2.73 (−0.02)	1.0 (49)
2OH	2.9 (203−243) 4.4 (243−293)	4.68	4.14	−4.76	−17.6	0.49 (−1.36)	30 (97)
3OH(1)[c]	15 (193−243) 4.6 (243−293)	4.87	1.86	−2.51	−13.9	1.63 (0.17)	6.0 (39)
3OH(2)[c]	3.2 (193−243) 4.6 (243−293)	4.72	4.10	−4.29	−16.0	0.47 (−1.21)	31 (96)

[a]Chemical shift for the hydroxyl proton(s). [b]Data at 298 and 193 K, and the latter is shown in parentheses. [c]**3OH**(1) and **3OH**(2) refer to the H-bonding mode of the **1OH**- and **2OH**-like hydroxyl groups in **3OH**.

DOI: 10.1021/acs.joc.5b02303
J. Org. Chem. 2015, 80, 12431−12443

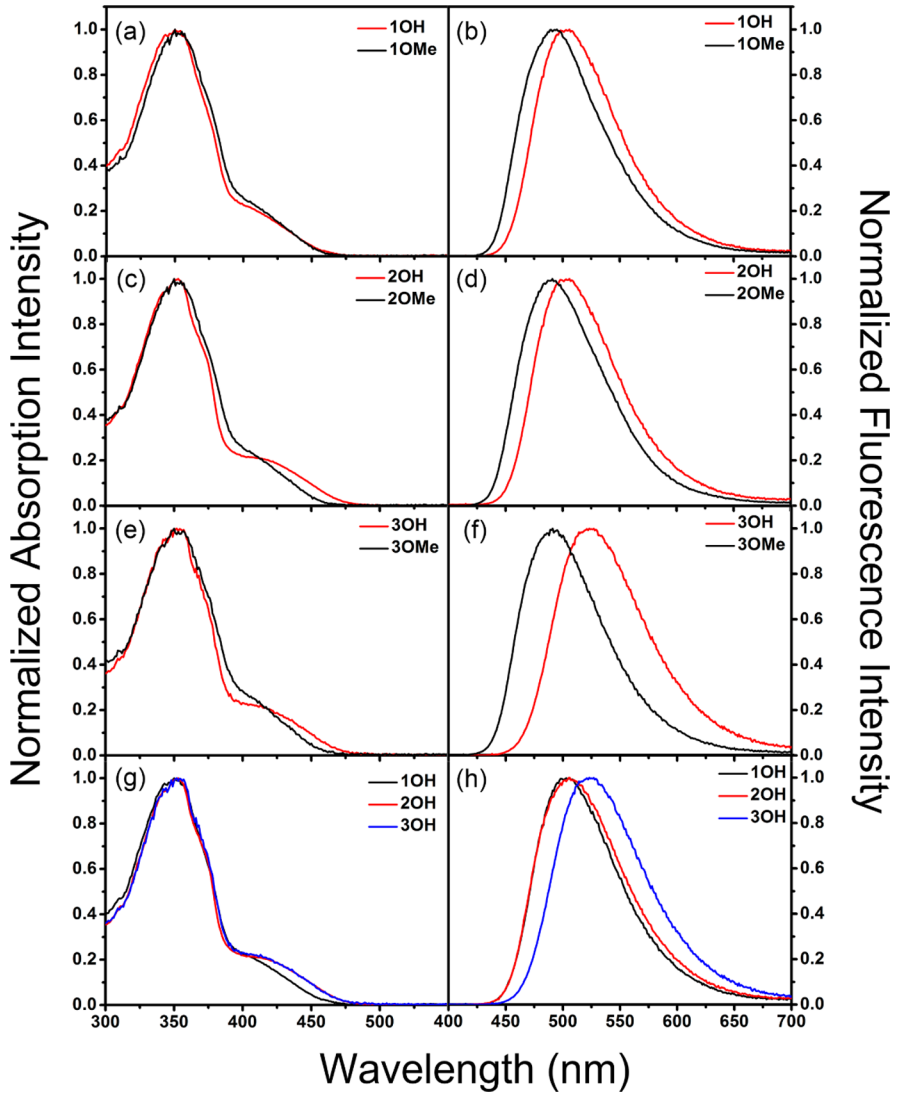

Figure 4. Electronic absorption and emission spectra of (a,b) **1OH** and **1OMe**, (c,d) **2OH** and **2OMe**, (e,f) **3OH** and **3OMe**, and (g,h) **1OH**−**3OH** in hexane (1×10^{-5} M).

Upon lowering the temperature from 298 to 128 K, **1OMe**−**3OMe** display a small enhancement of the intensity and slight modification of the spectral profile, which could be simply attributed to the temperature effect on solvent polarity and viscosity. In contrast, the spectra of **1OH**−**3OH** undergo stepwise variations, first like the cases of **1OMe**−**3OMe** with intensity enhancement but then being broadened with an intensity diminishment for the 350 nm band and a red shift for the 430 nm band. The turning temperature is the same (238 K) for **1OH** and **3OH** but lower (168 K) for **2OH**. In addition, the spectral broadening process ends at 198, 168, and 138 K for **1OH**, **3OH**, and **2OH**, respectively. Evidently, the H-bonding modes play a critical role in the observed temperature effect for **1OH**−**3OH**. Since entropy effect plays a role in forming either intra- or intermolecular H-bonds (Table 1), H-bonding interactions are expected to be more favorable at lower temperature. However, enhancement of H-bonding interactions alone could not explain the temperature-induced spectral broadening, because even the ubiquitous solute−solvent *intermolecular* C═O···H−O and C═N···H−O H-bonding for **1OH**−**3OH** in methanol did not lead to such a broad absorption spectrum (Figure S2). Instead, aggregate formation driven by intermolecular H-bonding interactions might facilitate intermolecular $\pi-\pi$ stacking interactions that are responsible for the spectral broadening. The degree of spectral broadening indeed agrees well with the relative tendency of forming intermolecular H-bonds: **1OH** > **3OH** > **2OH**; the turning and ceasing points of spectral changes correspond to the temperature at which aggregates start and end to form. The relationship **1OH** > **2OH** could be readily understood by the fact that the stronger is the intramolecular H-bond, the less is the availability of the OH group for forming intermolecular H-bond. The relationship **1OH** > **3OH** in the observed temperature effect indicates that the *intermolecular* C═N···H−O mode is more important than the C═O···H−O H-bonding mode in promoting aggregate formation, because the latter mode is available for both **1OH** and **3OH**, but the former is available only for **1OH**. That **3OH** > **2OH** on temperature-induced spectral broadening could be attributed to the formation of intermolecular C═O···H−O and/or H−O···H−O H-bonds in **3OH**; the latter H-bonding mode was observed in the crystals.

Fluorescence Spectra. The normalized fluorescence spectra of **1OH**−**3OH** relative to the corresponding non-H-

DOI: 10.1021/acs.joc.5b02303
J. Org. Chem. 2015, 80, 12431−12443

Table 2. Photophysical and Photochemical Data of 1OH−3OH and 1OMe−3OMe in Hexane (Hex), THF, and Acetonitrile (MeCN).[a]

compd	solvent	λ_{abs}[b] (nm)	λ_f (nm)	Φ_f	Φ_{ZE}[c]	τ_f[d] (ns)	k_r (10^8 s^{-1})	k_{nr} (10^8 s^{-1})
1OH[e]	Hex	352 (420)	506	0.43	nd	20.8	0.21	0.27
	THF	354 (429)	585	0.12	0.26	12.1	0.10	0.73
	MeCN	352 (431)	647[f]	0.02	0.17	2.8	0.07	3.50
1OMe[e]	Hex	352 (420)	491	0.45	nd	21.2	0.21	0.26
	THF	353 (427)	566[f]	0.13	0.42	14.7	0.09	0.59
	MeCN	353 (429)	632	0.04	0.40	7.9	0.05	1.22
2OH[e]	Hex	352 (424)	506	0.37	nd	18.9	0.20	0.33
	THF	356 (431)	585	0.11	0.27	13.2	0.08	0.67
	MeCN	355 (431)	639[f]	0.03	0.16	5.2	0.06	1.87
2OMe[e]	Hex	354 (422)	495	0.43	nd	22.4	0.19	0.25
	THF	355 (429)	569	0.14	0.47	15.3	0.09	0.56
	MeCN	355 (431)	632	0.06	0.44	7.7	0.08	1.22
3OH	Hex	352 (424)	523	0.38	nd	19.7	0.19	0.31
	THF	360 (429)	602	0.09	0.16	8.9	0.10	1.02
	MeCN	355 (429)	661	0.01	0.06	2.1	0.05	4.71
3OMe	Hex	350 (422)	491	0.45	nd	21.0	0.21	0.26
	THF	357 (429)	566	0.14	0.41	12.7	0.11	0.68
	MeCN	352 (431)	631	0.04	0.37	7.4	0.05	1.30

[a]Substrate concentration is 1×10^{-5} M for all data, except for Φ_{ZE}, which is 1×10^{-3} M. [b]Values in parentheses are the maxima. [c]For the purpose of solubility (1×10^{-3} M), MeCN solutions contain 20% THF for the measurement of Φ_{ZE}. Data are not determined (nd) in hexane because of poor solubility, even containing 20% THF. Excitation wavelength is 350 nm. [d]The τ_f was determined with excitation and emission around the spectral maxima. [e]Data from ref 30, unless otherwise noted. [f]Data revised in this work.

bonded species **1OMe−3OMe** in hexane are shown in Figure 4, and the data of fluorescence maximum (λ_{fl}) in hexane, THF, and MeCN are listed in Table 2. For all cases, the fluorescence maximum (λ_{fl}) undergoes red shifts by ∼140 nm from hexane to MeCN. Such a large solvatofluorochromicity indicates a strong charge-transfer character for the S_1 state of these *m*-DMABDIs.[30] Provided that the difference in λ_{fl} ($\Delta\lambda_{fl}$) between the H-bonded and non-H-bonded pairs reflects the electronic perturbation of H-bond on the S_1 state, the H-bonding effect is in the trend **3OH** (30−36 nm, 720−1250 cm^{-1}) > **1OH** (15−19 nm, 370−600 cm^{-1}) > **2OH** (7−16 nm, 170−480 cm^{-1}) in all three solvents.

The dependence of fluorescence spectra on temperature for **1OH−3OH** and **1OMe−3OMe** in MCH has been recorded in the temperature range 128−298 K with an interval of 10 K. Upon lowering the temperature from 298 to 128 K, all six compounds display an initial enhancement but then a diminishment of the fluorescence intensity and a red shift of λ_{fl}, but the extent is much larger for **1OH−3OH** than **1OMe−3OMe** (Figure 6). The intensity normalized spectra are shown in Figure S3. Comparison of the fluorescence intensity at 128 vs 298 K reveals that temperature-induced fluorescence quenching is largest for **3OH** and smallest for **2OH**. In line with the argument of aggregate formation for **1OH−3OH** but not for **1OMe−3OMe** at low temperatures based on VT absorption spectra (vide supra), the additional fluorescence quenching for the former relative to the latter compounds at low temperatures indicates the presence of other nonradiative decay channels induced by aggregate formation. Since aggregates involve with both $\pi-\pi$ stacking and intermolecular H-bonding interactions, it is interesting to evaluate their relative role in the observed fluorescence quenching. For the factor of $\pi-\pi$ stacking, the VT absorption spectra indicate a trend of **1OH** > **3OH** > **2OH** (vide infra), which does not fit with the relative size of fluorescence quenching **3OH** > **1OH** > **2OH**. On the other hand, the order of temperature-induced florescence quenching matches with the expected propensity of forming the C═O···H−O mode in the aggregates (**3OH** > **1OH** > **2OH**). In the following section, we will show that H-bonding to the carbonyl group is more important than to the imino group in quenching the excited state. Accordingly, we conclude that H-bonding interactions are more important than $\pi-\pi$ interactions in quenching the fluorescence of aggregates.

Quantum Yield and Lifetime. The quantum yields for fluorescence (Φ_f) and the Z → E photoisomerization (Φ_{ZE}) for the *m*-DMABDIs in hexane, THF, and/or MeCN at ambient temperature are provided in Table 2. Unlike most unconstrained GFP-like chromophores that display low Φ_f values in nonviscous solvents,[36,37] all the *m*-DMABDIs in hexane are strongly fluorescent (Φ_f = 0.37−0.45) and display a strong Φ_f dependence on the solvent polarity: the Φ_f is decreased by 1 order of magnitude on going from hexane to MeCN. According to the one-bond-flip mechanism for Z-E photoisomerization,[19,38−40] the probability of the τ torsion that leads to the *E* isomer is about 50%, and thus the quantum efficiency for the τ torsion is approximately equal to $2\Phi_{ZE}$. For the non-H-bonded species **1OMe−3OMe**, the observation of $\Phi_f + 2\Phi_{ZE} \approx 1.0$ (in the range 0.8−1.2 to accommodate the experimental uncertainty) in THF and MeCN indicates that fluorescence and the τ torsion are the main deactivation channels. In contrast,

DOI: 10.1021/acs.joc.5b02303
J. Org. Chem. 2015, 80, 12431−12443

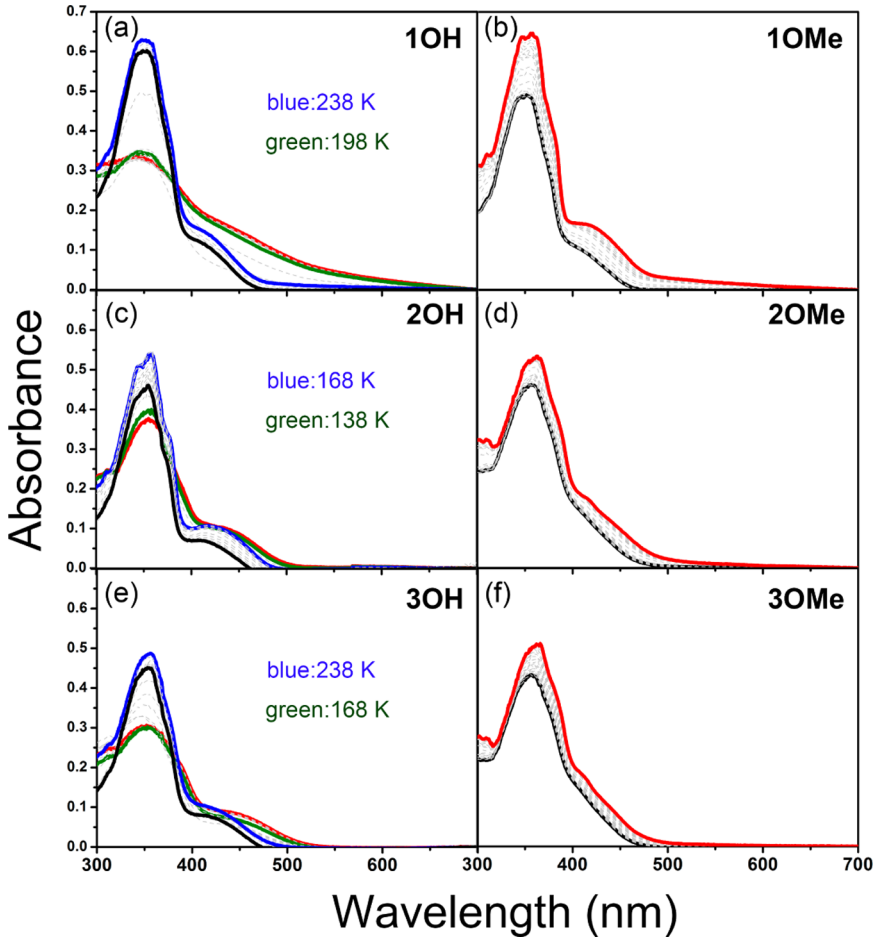

Figure 5. Electronic absorption spectra of (a) **1OH**, (b) **1OMe**, (c) **2OH**, (d) **2OMe**, (e) **3OH**, and (f) **3OMe** in methylcyclohexane (1×10^{-5} M) recorded in the temperature range 128−298 K with an interval of 10 K. The spectra were recorded from 298 K (black) to 128 K (red). For **1OH**−**3OH**, the spectra at the intensity-turning temperature are shown in blue and those at the end of temperature response are shown in green.

the sum $\Phi_f + 2\Phi_{ZE}$ is in the range ~0.1−0.6 for **1OH**−**3OH** in THF and MeCN, indicating the presence of other nonradiative decay channels and/or a strongly modified potential energy surface for the τ torsion owing to intramolecular H-bonding interactions.[27,28] The phenomenon of H-bond-induced excited-state quenching is also evidenced by the nearly complete fluorescence quenching for the *m*-DMABDIs in CH_3OH.[29−31]

The rate constants for the radiative (k_r) and nonradiative (k_{nr}) decays could be evaluated by the fluorescence quantum yields and lifetimes (τ_f) via eqs 5 and 6:

$$k_r = \Phi_f/\tau_f \quad (5)$$

$$k_{nr} = (1 - \Phi_f)/\tau_f \quad (6)$$

The data are listed in Table 2. All the fluorescence decay profiles can be well fit with a single exponential function. Like Φ_f, both the τ_f and k_r decrease with increasing the solvent polarity. The decrease of k_r in more polar solvents might indicate intensity borrowing of the lowest excited state from the higher excited states, as the energetic separation between the fluorescing state and the higher excited states of more allowed transition is larger in more polar solvents (Table 2). The difference in k_r between **1OH**−**3OH** and the corresponding non-H-bonded species **1OMe**−**3OMe** in the same solvent is negligible, revealing that the radiative transition rate is little perturbed by the intramolecular H-bond. In contrast, the difference in k_{nr} (Δk_{nr}) for the H-bonded vs non-H-bonded couple is substantial, particularly in more polar solvents (Figure 7). The Δk_{nr} is small ($(1-8) \times 10^6$ s^{-1}) in hexane but significant ($(0.7-3.4) \times 10^8$ s^{-1}) in MeCN for all the three pairs. Again, the Δk_{nr} can be attributed to the rate constant of H-bond-induced nonradiative decay (i.e., $k_{HB} = \Delta k_{nr}$). The observed H-bonding effect is in the order **3OH** > **1OH** > **2OH**.

The single exponential decay profiles recorded by the nanosecond time-correlated single photon counting apparatus for **1OH**−**3OH** in MeCN indicates that the H-bond-induced fluorescence quenching is either a diabatic process without forming any fluorescent intermediates or an adiabatic process having fluorescent products of lifetime shorter than the response time of our time-correlated single photon counting (TCSPC) apparatus. To clarify the situation, we have carried out femtosecond fluorescence up-conversion measurements on **1OH**−**3OH** and **1OMe**−**3OMe** in MeCN (1 mM). Figure 8 shows the time-resolved fluorescence decay profiles of **1OH**−**3OH** and **1OMe**−**3OMe** with excitation at 400 nm and probe at the peaks of the emission spectra. For all emission transient profiles presented here, the relaxation kinetics can be well described by a multiple exponential decay function containing three decay components with decay coefficients (τ_1, τ_2 and τ_3) on time scales of picoseconds, hundred picoseconds and nanoseconds; the corresponding fitted parameters are summarized in Table 3. Note that the same studies on the fluorescence decay profile of *m*-ABDI in MeCN can be well

DOI: 10.1021/acs.joc.5b02303
J. Org. Chem. 2015, 80, 12431−12443

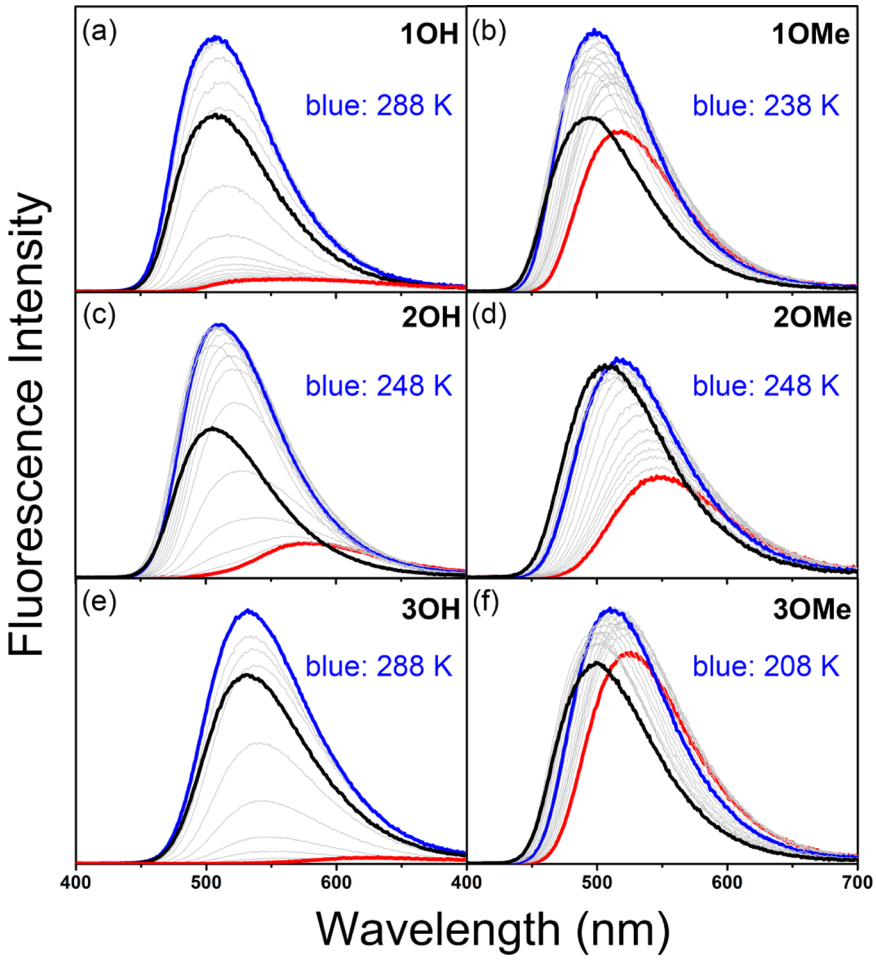

Figure 6. Fluorescence spectra of (a) **1OH**, (b) **1OMe**, (c) **2OH**, (d) **2OMe**, (e) **3OH**, and (f) **3OMe** in methylcyclohexane (MCH) recorded in the temperature range 128−298 K with an interval of 10 K. The spectra were recorded from 298 K (black) to 120 K (red) and the spectra of the highest intensity are shown in blue. Excitation wavelength is 350 nm.

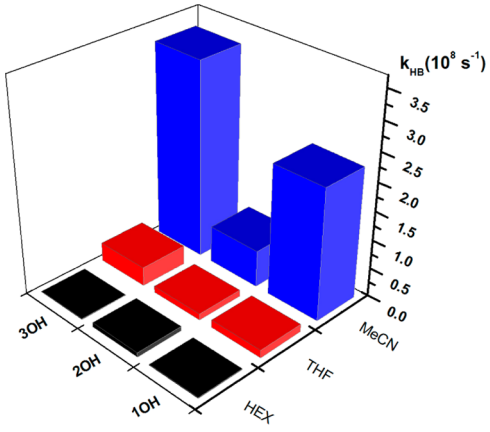

Figure 7. Comparison of k_{HB} (i.e., Δk_{nr}) for **1OH**−**3OH** in hexane, THF, and MeCN.

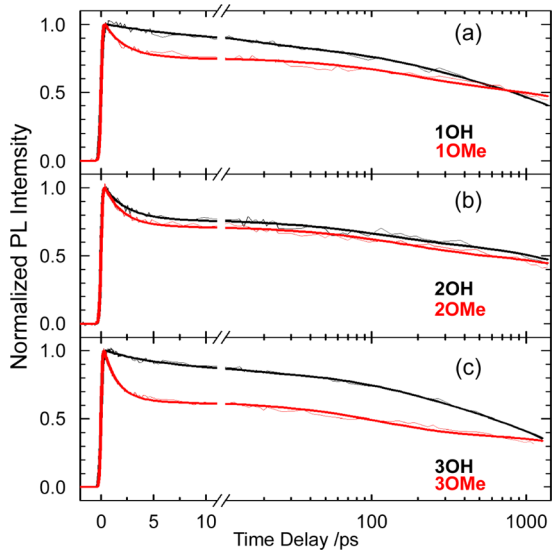

Figure 8. Normalized femtosecond fluorescence transients of (a) **1OH** and **1OMe**, (b) **2OH** and **2OMe**, and (c) **3OH** and **3OMe** in MeCN pumped at 400 nm and probed at the emission peaks as indicated in Table 3. The thin and thick traces are experimental data and fitting results, respectively.

described with a single exponential function on a time scale of nanoseconds.[28] Therefore, the additional picosecond and subnanosecond components (τ_1 and τ_2) observed for **1OH**−**3OH** and **1OMe**−**3OMe** relative to *m*-ABDI are associated with the presence of alkyl substituents. We assigned the fast-decay component (τ_1) to the Franck−Condon (FC) relaxation involving certain vibrational motions in the first excited state. The values of τ_1 of **1OH** and **3OH** are 4−5 times larger than

DOI: 10.1021/acs.joc.5b02303
J. Org. Chem. 2015, 80, 12431−12443

Table 3. Fluorescence Decay Time Coefficients (τ_1, τ_2 and τ_3) of 1OH−3OH and 1OMe−3OMe in MeCN with the Corresponding Relative Amplitudes Shown in Parentheses

compounds	λ_{em} (nm)	τ_1 (ps)	τ_2 (ps)	τ_3 (ns)
1OH	655	11.4 (0.14)	205 (0.20)	2.8 (0.66)
1OMe	630	2.0 (0.28)	184 (0.19)	7.9 (0.53)
2OH	640	2.1 (0.26)	108 (0.15)	5.2 (0.59)
2OMe	630	1.7 (0.33)	151 (0.17)	7.7 (0.50)
3OH	660	6.0 (0.15)	172 (0.20)	2.1 (0.65)
3OMe	630	1.4 (0.42)	112 (0.21)	7.4 (0.37)

those of **1OMe** and **3OMe**, indicating that the fast FC relaxation in the excited state is related to the hydroxyl groups. In other words, formation of the H-bonding of C═O···H−O in **1OH** and **3OH** retards this fast decay process in comparison to their counterparts (**1OMe** and **3OMe**). It is likely that formation of intramolecular C═O···H−O and/or intermolecular H-bonds in **2OH** is rather small such that the transient fluorescence profile of **2OH** is similar to that of **2OMe** (Figure 8b). The decay process with several hundred picoseconds (τ_2) may be assigned as an intrinsic relaxation process of these GFP-like chromophores showing similar relative amplitudes ($A_2 \sim 0.2$). The much slower relaxation kinetics in **1OH** and **3OH** than in **2OH** might result from their larger Stokes' shifts (Table 2). The ns-decay component (τ_3) has been assigned as the major internal conversion process observed also by the TCSPC measurements. The lack of new decay components for **1OH**−**3OH** vs **1OMe**−**3OMe** indicates that the H-bonding interactions do not produce observable intermediates in our fs fluorescence decay windows.

DISCUSSION

Ground-State H-Bonding. The ground-state H-bonding behavior of **1OH**−**3OH** has been investigated under a wide range of concentrations (form 10 μM to pure form) with electronic absorption and ^{1}H NMR spectroscopies and with X-ray crystallography. Figure 9 depicts the major H-bonding modes proposed for **1OH**−**3OH** in solutions of 1 mM concentration.

For **1OH**, we conclude that forming an *intermolecular* C═N···H−O H-bond (Figure 9a) is more favorable than the 7-membered *intramolecular* C═O···H−O counterpart (not shown). The preference of forming intermolecular rather than intramolecular H-bonds is evidenced by several observations, including the formation of aggregates (Figure 5) when the conformational entropy is diminished at low temperature, an upward curve of the chemical shift-temperature plot (Figure 3) with a large value of $-\Delta\delta/\Delta T$ (~39 ppb K^{-1}) in the low temperature range 203−243 K, and a significant H-bonding enthalpy ($\Delta H \approx 5.0$ kcal mol^{-1}, Table 1) that is inconsistent with a weak intramolecular C═O···H−O H-bond indicated by the absorption spectra (Figure 4). Regarding the nature of the *intermolecular* H-bonding, the C═N···H−O mode is expected to be more important than the C═O···H−O counterpart by three reasons: first, the imino nitrogen is inherently a better H-bond acceptor than the carbonyl oxygen;[23,41,42] second, the X-ray crystal structure of **1OH** displays such a H-bonding mode (Figure 1a); third, with the same type of hydroxyl group in **1OH** and **3OH**, the H-bonding behavior is quite different. More specifically, the carbonyl oxygen in both **1OH** and **3OH** is available for intermolecular H-bonding, but the imino nitrogen is accessible only in **1OH** but not in **3OH** because of its participation in intramolecular C═N···H−O H-bonding. Provided that the intermolecular C═O···H−O H-bonding was critical, the hydroxyl group in **1OH** and **3OH** should have had similar spectroscopic properties. However, this is not the case; the δ_{HB} (7.87 vs 4.87 ppm), ΔH (−5.0 vs −2.5 kcal mol^{-1}), and ΔS (−25.9 vs −13.9 cal mol^{-1}) are distinct in **1OH** vs **3OH**. In addition, the extent of spectral broadening at low temperature is larger for **1OH** than for **3OH** (Figure 5). Evidently, the C═N···H−O is the major intermolecular H-bonding mode. The thermodynamic parameters shown in Table 1 indicate that approximately half of the **1OH** molecules are H-bonded at 193 K, but at ambient temperature it is decreased to only about 1%.

The situation is different in the case of **2OH**, in which the 6-membered intramolecular C═N···H−O H-bond dominates (Figure 9b). This conclusion is supported by the low values of the reduced temperature constants ~2.9 and 4.4 ppb K^{-1} in both the low (203−243 K) and high (243−293 K) temperature range. Furthermore, the ^{1}H NMR-derived H-bond energy ~4.8 kcal mol^{-1} agrees satisfactorily with that (~5.7 kcal mol^{-1} in gas phase) predicted with DFT calculations.[30] The H-bonded form is about one-third at 293 K and increased to 97% at 193 K. This H-bonding mode must be energetically favorable such that it is retained in the solid state (Figure 1b).

The H-bonding behavior of **3OH** shows both analogies and differences as compared with **1OH** and **2OH**. For the sake of discussion, the two hydroxyl groups that correspond to the one in **1OH** and **2OH** are referred to **3OH**(1) and **3OH**(2), respectively. The H-bond with **3OH**(2) possesses a set of thermodynamic parameters similar to that in **2OH** (Table 1),

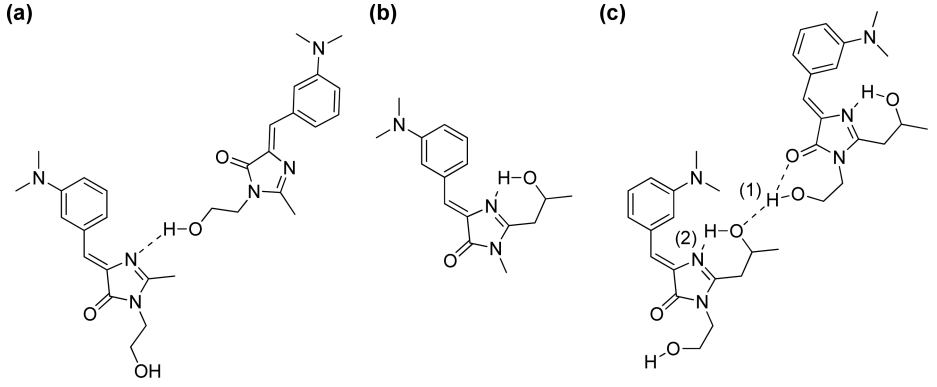

Figure 9. Major H-bonding mode proposed for (a) **1OH**, (b) **2OH**, and (c) **3OH** in solutions of 1 mM. The labels (1) and (2) in **3OH** correspond to those in Table 2.

DOI: 10.1021/acs.joc.5b02303
J. Org. Chem. 2015, 80, 12431−12443

revealing a conservation of the intramolecular C═N···H−O mode on going from **2OH** to **3OH**. In contrast, the thermodynamic and VT ^{1}H NMR data are significantly different for **3OH**(1) as compared to the one in **1OH**, indicating that the intermolecular C═N···H−O H-bonding mode is unimportant for the former. This conclusion is not unexpected, as the imino group in **3OH** participates in intramolecular H-bond and is no longer available for an intermolecular version. A clue to the H-bonding mode for **3OH**(1) is provided by the X-ray crystal structure (Figure 1c), in which an intermolecular H−O···H−O H-bond is formed. An engagement of intermolecular H-bond is consistent with a value of ∼15 ppb K^{-1} for the reduced temperature constant in the temperature range 193−233 K. However, the low values for both ΔS (−13.9 cal mol^{-1}) and $-\Delta\delta/\Delta T$ (∼4.6 ppb K^{-1}, 243−293 K) reveal the contribution of intramolecular H-bonding interactions, attributable to the intramolecular C═O···H−O mode. Collectively, the proposed H-bonding mode for **3OH** at 193 K is depicted in Figure 9c. This mixed inter- and intramolecular H-bonding mode for **3OH**(1) might account for the opposite trend in the H-bonded population on going from **1OH** to **3OH** at ambient vs low temperature: the population is increased (from 1 to 6%) at 298 K but decreased (from 49 to 39%) at 193 K. At ambient temperature, intermolecular H-bond is entropically unfavorable, and therefore the increase in H-bonded population should result from an enhancement of the intramolecular C═O···H−O H-bonding interactions. When the temperature is lowered, the contribution of the intermolecular H−O···H−O H-bond in **3OH** is increased but the effect is not as large as the C═N···H−O bonding in **1OH**, resulting in a decrease of H-bonded population for **3OH** vs **1OH**.

The increased tendency of forming 7-membered intramolecular C═O···H−O H-bond in **3OH** vs **1OH** indicates a cooperative effect between H-bonds: namely, the presence of the 6-membered intramolecular C═N···H−O H-bond in **3OH** enhances the neighboring 7-membered H-bond. Previous examples of H-bond cooperativity are divided into two categories, σ- and π-cooperativity.[1,43] An example of σ-cooperativity is ice, in which the H-bonds are connected by H−O σ-bonds. The H-bonds in π-cooperativity are linked by both the donor H−X σ-bond and the acceptor C═O or C═N π-bond, as exemplified by the H-bonded dimers of carboxylic acids. However, the cooperative effect in **3OH** does not fall into the typical patterns of σ- or π-bond cooperativity but could be rationalized by the polarization interactions: namely, polarization of the more stable 6-membered H-bond induces a polarization in the amido group and in turn the 7-membered H-bond as a result of increased negative charge density on the carbonyl oxygen (Figure 10).

In principle, the intermolecular H-bond for **1OH** and **3OH** would be entropically much less favorable when the substrate concentration is diluted by 100 times to 10 μM. This is supported by the lack of difference in the electronic absorption spectra of **1OH** and **1OMe** (Figure 4). Without the competition of forming intermolecular H-bond, the 7-membered C═O···H−O H-bonding interactions in **1OH** and **3OH** are expected to be enhanced. However, intermolecular H-bonding could be triggered again by lowering the temperature (e.g., 238 K), as evidenced by the aggregate formation (Figure 5).

In summary, the 6-membered intramolecular C═N···H−O H-bond in **2OH** and **3OH** is rather important, particularly in

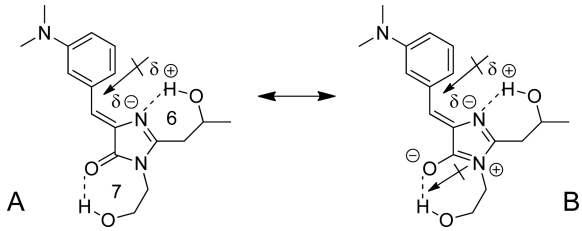

Figure 10. Schematic representation of the cooperativity of H-bonds in **3OH**: polarization of the 6-membered H-bond (resonance form A) enhances the polarization of the amido group (resonance form B) and thus the 7-membered H-bond.

nonpolar (hexane and MCH) and medium polar solvents (dichloromethane), but the 7-membered C═O···H−O H-bond is negligible or weak for **1OH** and **3OH** at ambient temperature, although a small enhancement is present for the latter owing to H-bond cooperative effect. When the conformational entropy is lowered at low temperature, the H-bonding mode for the ethanolic proton in **1OH** and **3OH** is dominated by intermolecular C═N···H−O or H−O···H−O rather than the intramolecular 7-membered C═O···H−O mode. These features are valid in both solutions and solid state. The minor role in H-bonding for the carbonyl group in **1OH**−**3OH** even in aggregates or crystals is intriguing in view of the fact that an amido carbonyl group is a well-documented H-bond acceptor in peptides and proteins as well as in many artificial systems.[33,34,44] This discrepancy could be attributed to the alcoholic H-bond donor; according to the crystallographic database, an isolated C═O···H−O H-bond is weak when it is not assisted by charges, resonance (π-cooperativity), or polarization (σ-cooperativity) interactions.[45]

Excited-State H-Bonding. The intramolecular H-bonding behavior of **1OH**−**3OH** (10 μM) in the lowest singlet excited state (S_1) has been characterized with steady-state and time-resolved fluorescence spectroscopies and by comparison with the non-H-bonded counterparts **1OMe**−**3OMe**.

One of the observed H-bonding effects on the excited state of **1OH**−**3OH** is the red shift of fluorescence maximum λ_{fl}. This phenomenon corresponds to a larger stabilization of the S_1 state relative to the ground state (S_0) by the H-bonding interactions, which can be understood by the charge-transfer character of the S_1 state of *m*-DMABDIs. Upon photoexcitation, charge transfer occurs from the amino donor to the imidazolinone acceptor, in which the electron density (basicity) for the C═N and C═O H-bond acceptors is enhanced (Figure 11). Consequently, a strengthening of the H-bond on going from S_0 to S_1 can be expected. This is particularly true for the intramolecular C═O···H−O H-bond, which is rather weak in S_0 but becomes significant in S_1, as evidenced by the negligible vs significant spectral shift of the absorption vs fluorescence spectra for **1OH** relative to **1OMe** in hexane at ambient temperature (Figure 4). In the case of ground-state H-bonded systems such as **2OH**, H-bonding interactions in the electron-accepting group would increase the electron-pulling ability of the H-bond acceptor and thus enhance the charge-transfer character, which shifts both the absorption and fluorescence bands to longer wavelength. The similar extent of red shift in the absorption and fluorescence profiles for **2OH** vs **2OMe** indicate a small or negligible change of the intramolecular C═N···H−O H-bonding strength on going from S_0 to S_1. Regarding the size of H-bond-induced fluorescence shift ($\Delta\lambda_{fl}$), it is much larger for **3OH** than for

DOI: 10.1021/acs.joc.5b02303
J. Org. Chem. 2015, 80, 12431−12443

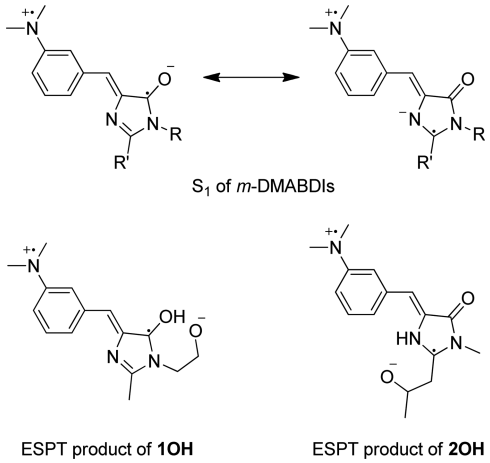

Figure 11. Schematic representation of the charge-transfer S_1 state and the excited-state proton transfer (ESPT) product of *m*-DMABDIs.

1OH and **2OH** (Table 2). The cooperative effect of the two H-bonds in the S_1 state of **3OH** is evidenced by the relationship of **3OH** > **1OH** + **2OH** in the size of $\Delta\lambda_{fl}$ (~1250 vs 1040 cm^{-1}) in hexane, in which fluorescence quenching is minimal and the value of $\Delta\lambda_{fl}$ reflects the size of H-bonding interactions. A comparison of the excited-state H-bonding effect on λ_{abs} and λ_{fl} for **1OH**−**3OH** in hexane is schematically shown in Figure 12.

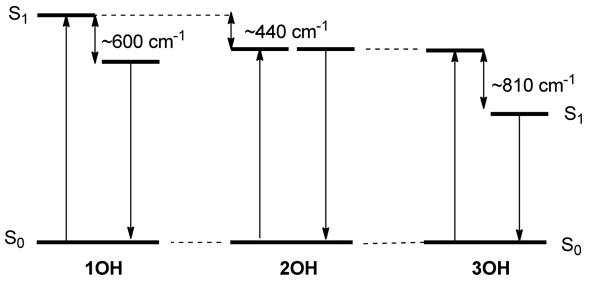

Figure 12. Schematic representation of the H-bonding effect on the absorption and emission of **1OH**−**3OH** in hexane.

The fluorescence spectral broadening observed for **1OH** but not for **2OH** at low temperatures (Figure S3) deserves a comment. Since the latter does not involve with aggregation but simply with increased population of intramolecularly H-bonded form upon lowering the solution temperature, the spectral broadening in the former should be a consequence of intermolecular π,π-interactions due to aggregate formation. For comparison, the presence of both intramolecular C═N···H−O and intermolecular H−O···H−O H-bonds in **3OH** gives rise to a red-shifted and less broadened spectrum at low temperature.

Another observed excited-state H-bonding effect is fluorescence quenching. There are several possible mechanisms for H-bond-induced fluorescence quenching: internal conversion,[5,7,8] electron transfer,[6,10,11] proton transfer,[23] and coupled electron−proton transfer.[8] Provided that vibronic coupling to the ground state via H-bond were responsible for **1OH**−**3OH**, the fluorescence quenching should be more significant in less polar solvents, because the population of H-bonded form generally increases with decreasing the solvent polarity.[46] This expectation is contradictory to the observations, in which the H-bonding effect is larger in more polar solvents (Figure 7). As for the possibility of H-bond-induced electron transfer, a good electron donor such as amines is generally required.[6,11,46,47] Nevertheless, the possibility of phenols[7,10] and aliphatic alcohols[12] being electron donors for H-bond-induced electron transfer has also been proposed. While we cannot completely exclude the involvement of electron transfer in the fluorescence quenching of **1OH**−**3OH**, the ESPT mechanism is more likely to be responsible in several respects. First, aliphatic alcohols are inherently poor electron donors for photoinduced electron transfer.[47] Second, more electron-deficient BDI derivatives such as **5** and **6** (Chart 2) should be better electron acceptors than

Chart 2

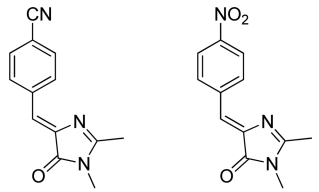

1OH−**3OH**, but the formers do not display fluorescence quenching in alcohols.[36] Third, our previous femtosecond transient fluorescence and infrared spectroscopic studies on *m*-ABDI in methanol supports the presence of proton transfer intermediates.[28] In addition, both diabatic and adiabatic ESPT have been observed for *m*-HBDI.[23] The solvent effect on fluorescence quenching is also consistent with the formation of polar zwitterionic products of ESPT, which is better stabilized in more polar solvents (Figure 11). Finally, the site-selectivity of H-bond-induced fluorescence quenching is better explained with the excited-state basicity of the H-bond acceptors. The absence of fluorescent intermediates in the femtosecond up-conversion experiments indicates a diabatic proton transfer process in **1OH**−**3OH**.[22,23]

Further comparison of the k_{HB} values for **1OH**−**3OH** sheds light on the relative efficiency of the two H-bonding modes on the fluorescence quenching. The k_{HB} of **2OH** is the smallest among **1OH**−**3OH** (**3OH** > **1OH** > **2OH**), despite the favorable intramolecular C═N···H−O H-bonding interactions in the ground state. In addition, the k_{HB} for **3OH** in THF (0.34×10^{-8} s^{-1}) and MeCN (3.41×10^{-8} s^{-1}) is larger than the sum of k_{HB} for **1OH** and **2OH** in the same solvents (0.25×10^{-8} s^{-1} in THF and 2.95×10^{-8} s^{-1} in MeCN) by 15−36%. Evidently, the C═O···H−O H-bonding mode plays a more important role than the C═N···H−O one in quenching the excited state, and the H-bond cooperativity in **3OH** is effective on fluorescence quenching as well as on fluorescence spectral shift (vide supra). An increase of the C═O···H−O H-bonding interactions in S_1 vs S_0 could be understood by the increased electron density (basicity) for the carbonyl oxygen in the excited state as a result of intramolecular charge transfer. In addition, a lifetime in the nanosecond time scale is sufficient for the excited state to reach equilibration between the H-bonded and non-H-bonded states. It should be noted that fluorescence quenching due to the C═O···H−O H-bonding interactions has not been observed for the other GFP-like chromophores except for the *m*- and *o*-amino derivatives.[19,28−30] We believe that both the strong charge-transfer character and the long lifetime for the S_1 state are required to have such a fluorescence quenching channel.

The structural aspect of excited-state H-bonding effect also deserves a comment. Previous work by Inoue and co-workers

DOI: 10.1021/acs.joc.5b02303
J. Org. Chem. 2015, 80, 12431−12443

on aminoquinones and aminofluorenones has led to a hypothesis that the H-bond located on the same plane of the C═O group (in-plane mode) does not quench the excited state but lowers the fluorescence energy and it is the one perpendicular to the plane of the C═O group (out-of-plane mode) responsible for the fluorescence quenching.[5] This argument might also apply to **1OH**−**3OH**, which display both fluorescence shifts and quenching relative to the non-H-bonded **1OMe**−**3OMe**.

CONCLUSION

On the basis of variable-temperature electronic and ^{1}H NMR spectroscopies and X-ray crystallography, the H-bonding behavior of **1OH**−**3OH** in the ground and excited states are elucidated. The 7-membered C═O···H−O intramolecular H-bond is rather weak in the ground state but becomes significant in the lowest singlet excited state because of enhanced basicity in the H-bond acceptors and sufficiently long excited-state lifetimes for equilibration. In contrast, the 6-membered C═N···H−O intramolecular H-bond is favorable in both the ground and excited states. When the temperature is lowered or the substrate concentration is increased, intermolecular H-bonding interactions of several possible modes become important and could induce the formation of aggregates. The C═O···H−O H-bonding mode plays the major role in the fluorescence quenching. H-bond cooperativity in **3OH** is manifested, and to the best of our knowledge it provides the first example of excited-state H-bond cooperativity on fluorescence quenching. We have recently shown that H-bond responsive fluorophores are potential fluorescence turn-on dyes for cell imaging.[31] The site-selectivity and cooperativity of H-bonds reported in this work should be valuable for the design of novel GFP-like chromophores as fluorescent probes or imaging dyes.

EXPERIMENTAL SECTION

General Methods. NMR spectra were determined with a 500 or 400 MHz spectrometer using 5 mm gradient TBI and TBO probes, respectively. The chemical shifts for ^{1}H and ^{13}C spectra were referenced to the signals of chloroform-d_1 ($\delta(^1H)$ = 7.24 and $\delta(^{13}C)$ = 77.0), or DMSO-d_6 ($\delta(^1H)$ = 2.5 and $\delta(^{13}C)$ = 39.5). For the variable-temperature experiments, the temperature was well calibrated by ^{1}H signals of ethylene glycol and methanol such that the temperature error was within ±1 K. FID signals were acquired after a sufficient temperature equilibration time (10−15 min). High-resolution mass data were obtained with an ESI-TOF instrument.

Electronic Spectra. The steady-state and time-resolved instruments and experimental methods are the same as those described in the previous publications.[27,28] VT absorption and emission spectra were recorded with the sample in an cryostat equipped with an temperature controller for the measurements in the range 128−298 K. The sample in each temperature was allowed to reach thermal equilibrium for 10 min.

Photoisomerization Quantum Yield. Quantum yield of photoisomerization were measurement with optically dense degassed solution (~1 × 10^{-3} M) under 350 nm light irradiation of a 75-W Xe arc lamp equipped with monochromaters. The reference standard was *trans*-4-(*N*-phenylamino)stilbene (Φ_{tc} = 0.34 in CH_2Cl_2).[48] The extent of photoisomerization (less than 10%) was determined by HPLC without back reaction correction. The $Z \rightarrow E$ isomerization quantum yield (Φ_{ZE}) was calculated according to eq 7:

$$\frac{C_1 \times V_1 \times P_1}{\Phi_{ZE} \times t_1} = \frac{C_2 \times V_2 \times P_2}{\Phi_{tc} \times t_2} \quad (7)$$

where the subscripts 1 and 2 denote the concentration of sample and standard, respectively; C is the concentration; V is the volume; P is the amount (%) of *trans* → *cis* or $Z \rightarrow E$ conversion, t is the irradiation time; Φ_{tc} is the isomerization quantum yield of the standard. The reproducibility error is within 10% of the average.

X-ray Crystallography. Single crystals of **3OH** were obtained by slow crystallization in a mixed solvent of ethyl acetate and hexane in the dark to avoid the Z → E photoisomerization. The X-ray crystal structures were determined by a CCD diffractometer quipped with graphite-monochromated Mo Kα radiation (λ = 0.71073 Å) at 200 K. The previously reported[30] crystal structures of **1OH** and **2OH** have been refined and the revised crystallographic data, thermal ellipsoid plots, and unit cells along with those of **3OH** are reported in Table S1 and Figures S4−S9. The cif files of **1OH** (CCDC 1420284, ic13896), **2OH** (CCDC 1420285, ic13901) and **3OH** (CCDC 1415005, ic16612) have been deposited to The Cambridge Crystallographic Data Centre.

Materials. All solvents and materials for synthesis were reagent grade and commercially available without further purification, unless otherwise noted. Anhydrous dichloromethane (DCM) was used from the solvent purifier. The moisture content was less than 10 ppm.

Synthesis of 4. In a 50 mL sealed tube, **1OMe** (0.60 g, 2.09 mmol) and acetaldehyde (6.0 mL, 0.11 mol) were added. The mixture was heated for 21 h at 130 °C. After cooling to room temperature, the tube was opened (caution!!) and the solution was transferred to a single-neck flask in an ice bath. The residue was concentrated under reduced pressure and extracted with DCM/H_2O. The organic phase was dried with anhydrous $MgSO_4$ and concentrated again under reduced pressure. Purification was carried out by column chromatography on Al_2O_3 with DCM/EA (5:1) as eluent to provide yellow solid of **4** (0.20 g, 0.606 mmol) in 29% yield. mp: 100.0−101.3 °C; ^{1}H NMR (400 MHz, $CDCl_3$) δ: 1.34 (d, J = 6.4 Hz, 3H), 2.63−2.81 (m, 2H), 2.97 (s, 6H), 3.29 (s, 3H), 3.51 (t, J = 4.8 Hz, 2H), 3.74 (t, J = 4.8 Hz, 2H), 4.42 (m, 1H), 4.73 (s, 1H), 6.78 (d, J = 4.0 Hz, 1H), 6.92 (s, 1H), 7.10 (s, 1H), 7.25 (s, 1H), 7.27 (s, 1H), 7.61 (s, 1H); ^{13}C NMR (100 MHz, $CDCl_3$) δ: 22.5, 36.6, 40.6, 40.7, 59.0, 64.4, 70.5, 115.2, 115.5, 121.2, 129.0, 129.3, 134.4, 136.8, 150.5, 165.0, 170.1; IR (KBr): 3433, 2925, 2854, 2810, 1710, 1641, 1597, 1436, 1120, 999, 779 cm^{-1}; HRMS (ESI$^+$): calcd. for $C_{18}H_{25}N_3NaO_3^+$ (M+Na$^+$), 354.1788; found, 354.1796.

Synthesis of 3OMe. In a 10 mL round-bottom flask, **4** (50 mg, 0.15 mmol) was dissolved in 20 mL MeOH, 2.5 mL 37% HCl was then added to the solution, and the mixture was allowed to react for 48 h at room temperature. The reaction was quenched by neutralization (pH 7) with 10% $NaOH_{(aq)}$ in the ice bath. The solution was concentrated under reduced pressure, and the residue was subjected to extraction with DCM/H_2O. The organic phase was dried with anhydrous $MgSO_4$ and concentrated under reduced pressure. Column chromatography on silica gel with HXN/DCM/EA (4:5:1) as eluent afforded the desired **3OMe** as yellow powder (31 mg, 0.09 mmol) in 66% yield. mp: 90.7−92.3 °C; ^{1}H NMR (400 MHz, $CDCl_3$) δ: 1.33 (d, J = 6.0 Hz, 3H), 2.67−2.73 (m, 2H), 2.97 (s, 6H), 3.29 (s, 3H), 3.35 (s, 3H), 3.50 (t, J = 5.2 Hz, 2H), 3.79 (t, J = 5.2 Hz, 2H), 4.00 (m, 1H), 6.77 (d, J = 6.0 Hz, 1H), 7.06 (s, 1H), 7.24−7.30 (m, 2H), 7.40 (d, J = 7.4 Hz, 1H), 7.73 (s, 1H); ^{13}C NMR (100 MHz, $CDCl_3$) δ: 14.1, 19.6, 29.7, 35.7, 40.5, 40.6, 56.5, 58.9, 70.6, 74.6, 114.8, 116.0, 121.3, 128.4, 129.2, 134.8, 138.2, 150.7, 163.5, 171.0; IR (KBr): 2958, 2925, 2854, 1708, 1642, 1596, 1436, 1123, 999, 778 cm^{-1}; HRMS (ESI$^+$): calcd. for $C_{19}H_{28}N_3O_3^+$ (M+H$^+$), 346.2125; found, 346.2117.

Synthesis of 3OH. Compound **4** (150 mg, 0.45 mmol) was put under vacuum for 30 min in a 25 mL Schlenk flask, and then 15 mL dried DCM was added to the flask under nitrogen atmosphere. In an ice bath, the mixture was added BBr_3 (0.04 mL, 0.41 mmol) over a period of 30 min. The mixture was allowed to react at room temperature for 2 h. The reaction was then quenched by neutralization (pH 7) with sat. $NaHCO_{3(aq)}$ followed by extraction with DCM/H_2O. The organic phase was dried with anhydrous $MgSO_4$ and concentrated under reduced pressure. Column chromatography on silica gel with DCM/EA/MeOH (70:25:5) as eluent afforded **3OH** as yellow solid (84 mg, 0.26 mmol) in 59% yield. mp: 125.4−126.8 °C; ^{1}H NMR

DOI: 10.1021/acs.joc.5b02303
J. Org. Chem. 2015, 80, 12431−12443

(400 MHz, DMSO-d_6) δ: 1.24 (d, J = 6.0 Hz, 3H), 2.73−2.86 (m, 2H), 2.92 (s, 6H), 3.49−3.54 (m, 2H), 3.64−3.71 (m, 2H), 4.18−4.27 (m, 1H), 4.87 (d, J = 4.5 Hz, 1H), 4.94 (t, J = 5.6 Hz, 1H), 6.79 (dd, J = 8.4 Hz and J = 2.4 Hz, 1H), 6.92 (s, 1H), 7.24 (t, J = 8.0 Hz, 1H), 7.43 (d, J = 7.6 Hz, 1H), 7.72 (s, 1H); ^{13}C NMR (100 MHz, DMSO-d_6) δ: 23.9, 38.2, 43.2, 59.3, 64.8, 114.8, 116.0, 120.9, 126.4, 129.5, 135.0, 138.6, 150.9, 165.7, 170.5; IR (KBr): 3402, 2973, 2884, 2810, 1715, 1648, 1598, 1433, 1353, 1138, 779 cm^{-1}; HRMS (ESI$^+$): calcd. for $C_{17}H_{24}N_3O_3^+$ (M+H$^+$), 318.1812; found, 318.1808.

■ ASSOCIATED CONTENT

Supporting Information

The Supporting Information is available free of charge on the ACS Publications website at DOI: 10.1021/acs.joc.5b02303.

Thermal ellipsoid plots, and unit cells, electronic spectra, and ^{1}H and ^{13}C spectra of new compounds (PDF)
Crystallographic data (CIF)

■ AUTHOR INFORMATION

Corresponding Author

*E-mail: jsyang@ntu.edu.tw.

Notes

The authors declare no competing financial interest.

■ ACKNOWLEDGMENTS

We thank the Ministry of Science and Technology, Taiwan, and National Taiwan University (104R891303) for financial support, Mr. Che-Jen Lin (NTU, Taiwan) for technical assistance on electronic spectroscopy, and Prof. Chetti Prabhakar (National Institute of Technology, India) for helpful discussions.

■ REFERENCES

(1) Steiner, T. *Angew. Chem., Int. Ed.* **2002**, *41*, 48−76.
(2) González-Rodríguez, D.; Schenning, A. P. H. J. *Chem. Mater.* **2011**, *23*, 310−325.
(3) Such, G. K.; Johnston, A. P. R.; Caruso, F. *Chem. Soc. Rev.* **2011**, *40*, 19−29.
(4) (a) Zhao, G.-J.; Han, K.-L. *Acc. Chem. Res.* **2012**, *45*, 404−413. (b) Deng, F.; Kubin, J.; Testa, A. C. *J. Photochem. Photobiol., A* **1998**, *118*, 1−6. (c) Zhao, G.-J.; Han, K.-L. *ChemPhysChem* **2008**, *9*, 1842−1846.
(5) (a) Morimoto, A.; Yatsuhashi, T.; Shimada, T.; Kumazaki, S.; Yoshihara, K.; Inoue, H. *J. Phys. Chem. A* **2001**, *105*, 8840−8849. (b) Morimoito, A.; Yatsuhashi, T.; Shimada, T.; Biczók, L.; Tryk, D. A.; Inoue, H. *J. Phys. Chem. A* **2001**, *105*, 10488−10496.
(6) Herbich, J.; Kijak, M.; Zielińska, A.; Thummel, R. P.; Waluk, J. *J. Phys. Chem. A* **2002**, *106*, 2158−2163.
(7) Zhao, G.-J.; Han, K.-L. *J. Phys. Chem. A* **2007**, *111*, 9218−9223.
(8) Biczók, L.; Bérces, T.; Linschitz, H. *J. Am. Chem. Soc.* **1997**, *119*, 11071−11077.
(9) (a) Tolbert, L. M.; Solntsev, K. M. *Acc. Chem. Res.* **2002**, *35*, 19−27. (b) El Nahhas, A.; Pascher, T.; Leone, L.; Panzella, L.; Napolitano, A.; Sundström, V. *J. Phys. Chem. Lett.* **2014**, *5*, 2094−2100.
(10) Barman, N.; Singha, D.; Sahu, K. *J. Phys. Chem. A* **2013**, *117*, 3945−3953.
(11) Barman, N.; Singha, D.; Sahu, K. *Phys. Chem. Chem. Phys.* **2014**, *16*, 6159−6166.
(12) Zhao, G.-J.; Liu, J.-Y.; Zhou, L.-C.; Han, K.-L. *J. Phys. Chem. B* **2007**, *111*, 8940−8945.
(13) Wang, D.; Zhao, G.-J. *Commun. Comput. Chem.* **2013**, *1*, 181−190.
(14) Zimmer, M. *Chem. Rev.* **2002**, *102*, 759−782.
(15) Meech, S. R. *Chem. Soc. Rev.* **2009**, *38*, 2922−2934.
(16) Tolbert, L. M.; Baldridge, A.; Kowalik, J.; Solntsev, K. M. *Acc. Chem. Res.* **2012**, *45*, 171−181.
(17) Niwa, H.; Inouye, S.; Hirano, T.; Matsuno, T.; Kojima, S.; Kubota, M.; Ohashi, M.; Tsuji, F. I. *Proc. Natl. Acad. Sci. U. S. A.* **1996**, *93*, 13617−13622.
(18) Altoe', P.; Bernardi, F.; Garavelli, M.; Orlandi, G.; Negri, F. *J. Am. Chem. Soc.* **2005**, *127*, 3952−3963.
(19) Yang, J.-S.; Huang, G.-J.; Liu, Y.-H.; Peng, S.-M. *Chem. Commun.* **2008**, 1344−1346.
(20) Chattoraj, M.; King, B. A.; Bublitz, G. U.; Boxer, S. G. *Proc. Natl. Acad. Sci. U. S. A.* **1996**, *93*, 8362−8367.
(21) Stoner-Ma, D.; Jaye, A. A.; Matousek, P.; Towrie, M.; Meech, S. R.; Tonge, P. J. *J. Am. Chem. Soc.* **2005**, *127*, 2864−2865.
(22) Dong, J.; Solntsev, K. M.; Poizat, O.; Tolbert, L. M. *J. Am. Chem. Soc.* **2007**, *129*, 10084−10085.
(23) Solntsev, K. M.; Poizat, O.; Dong, J.; Rehault, J.; Lou, Y.; Burda, C.; Tolbert, L. M. *J. Phys. Chem. B* **2008**, *112*, 2700−2711.
(24) Chen, K.-Y.; Cheng, Y.-M.; Lai, C.-H.; Hsu, C.-C.; Ho, M.-L.; Lee, G.-H.; Chou, P.-T. *J. Am. Chem. Soc.* **2007**, *129*, 4534−4535.
(25) Hsieh, C.-C.; Chou, P.-T.; Shih, C.-W.; Chuang, W.-T.; Chung, M.-W.; Lee, J.; Joo, T. *J. Am. Chem. Soc.* **2011**, *133*, 2932−2943.
(26) Chuang, W.-T.; Hsieh, C.-C.; Lai, C.-H.; Lai, C.-H.; Shih, C.-W.; Chen, K.-Y.; Hung, W.-Y.; Hsu, Y.-H.; Chou, P.-T. *J. Org. Chem.* **2011**, *76*, 8189−8202.
(27) Huang, G.-J.; Cheng, C.-W.; Hsu, H.-Y.; Prabhakar, C.; Lee, Y.-P.; Diau, E. W.-G.; Yang, J.-S. *J. Phys. Chem. B* **2013**, *117*, 2695−2704.
(28) Cheng, C.-W.; Huang, G.-J.; Hsu, H.-Y.; Prabhakar, C.; Lee, Y.-P.; Diau, E. W.-G.; Yang, J.-S. *J. Phys. Chem. B* **2013**, *117*, 2705−2716.
(29) Huang, G.-J.; Lin, C.-J.; Liu, Y.-H.; Peng, S.-M.; Yang, J.-S. *Photochem. Photobiol.* **2015**, *91*, 714−722.
(30) Huang, G.-J.; Ho, J.-H.; Prabhakar, C.; Liu, Y.-H.; Peng, S.-M.; Yang, J.-S. *Org. Lett.* **2012**, *14*, 5034−5037.
(31) Tou, S.-L.; Huang, G.-J.; Chen, P.-C.; Chang, H.-T.; Tsai, J.-Y.; Yang, J.-S. *Chem. Commun.* **2014**, *50*, 620−622.
(32) Bernet, B.; Vasella, A. *Helv. Chim. Acta* **2000**, *83*, 995−1021.
(33) Gellman, S. H.; Dado, G. P.; Liang, G. B.; Adams, B. R. *J. Am. Chem. Soc.* **1991**, *113*, 1164−1173.
(34) Gung, B. W.; MacKay, J. A.; Zou, D. *J. Org. Chem.* **1999**, *64*, 700−706.
(35) Lämmermann, A.; Szatmári, I.; Fülöp, F.; Kleinpeter, E. *J. Phys. Chem. A* **2009**, *113*, 6197−6205.
(36) Lee, J.-S.; Baldridge, A.; Feng, S.; SiQiang, Y.; Kim, Y. K.; Tolbert, L. M.; Chang, Y.-T. *ACS Comb. Sci.* **2011**, *13*, 32−38.
(37) Ivashkin, P. E.; Yampolsky, I. V.; Lukyanov, K. A. *Russ. J. Bioorg. Chem.* **2009**, *35*, 652−669.
(38) Saltiel, J.; Charlton, J. *Rearrangements in Ground and Excited States*; de Mayo, P., Ed.; Academic Press: New York, 1980; p 25.
(39) Görner, H.; Kuhn, H. J. *Adv. Photochem.* **1995**, *19*, 1−117.
(40) Huang, G.-J.; Yang, J.-S. *Chem. - Asian J.* **2010**, *5*, 2075−2085.
(41) El Yazal, J.; Prendergast, F. G.; Shaw, D. E.; Pang, Y.-P. *J. Am. Chem. Soc.* **2000**, *122*, 11411−11415.
(42) Stavrov, S. S.; Solntsev, K. M.; Tolbert, L. M.; Huppert, D. *J. Am. Chem. Soc.* **2006**, *128*, 1540−1546.
(43) Jeffrey, G. A. *Crystallogr. Rev.* **1995**, *4*, 213−254.
(44) Wilson, S. O.; Tran, N. T.; Franz, A. K. *Organometallics* **2012**, *31*, 6715−6718.
(45) Gilli, G.; Gilli, P. *J. Mol. Struct.* **2000**, *552*, 1−15.
(46) Ikeda, N.; Miyasaka, H.; Okada, T.; Mataga, N. *J. Am. Chem. Soc.* **1983**, *105*, 5206−5211.
(47) Ghosh, H. N.; Adamczyk, K.; Verma, S.; Dreyer, J.; Nibbering, E. T. *Chem. - Eur. J.* **2012**, *18*, 4930−4937.
(48) Yang, J.-S.; Liau, K.-L.; Wang, C.-M.; Hwang, C.-Y. *J. Am. Chem. Soc.* **2004**, *126*, 12325−12335.

DOI: 10.1021/acs.joc.5b02303
J. Org. Chem. 2015, 80, 12431−12443